Available online at www.sciencedirect.com
ScienceDirect
Trans. Nonferrous Met. Soc. China 33(2023) 1054−1065
Transactions of Nonferrous Metals Society of China
www.tnmsc.cn

Mechanical and tribological behaviour of Al−Mg−$Cu_{(p)}$ composite cladded on AA1050 substrate

Hamed JAMSHIDI AVAL

Department of Materials Engineering, Babol Noshirvani University of Technology, Shariati Avenue, Babol 47148-71167, Iran

Received 7 December 2021; accepted 8 July 2022

Abstract: The effect of adding copper powder and changing the rotational speed of the consumable rod during friction surfacing of Al−Mg alloy on AA1050 aluminum substrate was investigated. The copper powder was inserted by drilling holes in the cross-section of the consumable rod. The coating microstructure was studied using optical and electron microscopy, and the mechanical properties of coatings were studied using a shear test. The results showed that with increasing the rotational speed of the consumable rod from 600 to 1000 r/min, the copper powder distribution becomes more uniform, and the agglomeration of copper powder occurs less frequently. The average grain size of coatings decreased from (2.0±0.1) to (0.9±0.2) μm by increasing the rotational speed from 600 to 1000 r/min. As the rotational speed increases, the copper-rich particles become smaller and are formed as $CuAl_2$ intermetallic compounds. The maximum load required for debonding coating from substrate increases from 16.2 to 18.4 kN by increasing rotational speed from 600 to 1000 r/min. The coating with rotational speeds of 600, 800, and 1000 r/min results in 12%, 18%, and 21% lower wear rate than that of the AA1050 substrate, respectively.

Key words: friction surfacing; Al−Mg matrix composite; copper reinforcement; mechanical property; AA1050 substrate

1 Introduction

Surface engineering is designed to protect the surface layer against corrosion, wear, oxidation, and similar factors. Many methods, such as laser and plasma coating, are used to coat aluminum alloys, but these methods usually have limited applications and are not economically viable. Due to the disadvantages and limitations of fusion methods, attention has been drawn to solid-state methods. Because these methods occur below the melting temperature of the material, they do not have the disadvantages of fusion methods such as cracks and cavities [1]. Solid-state methods include processes such as friction surfacing (FS). In FS, similar and dissimilar metals are joined by a strong metallurgical-mechanical bond, and a fine-grained structure with high strength is created. The FS method consists of three primary parameters: traverse speed, rotation speed, and axial feeding rate of the consumable rod. The geometric and mechanical properties of the coating can be controlled by changing these parameters. In the FS method, due to severe plastic deformation (SPD) and the heat generated due to friction, dynamic recrystallization (DRX) occurs both continuously and discontinuously in the microstructure. The FS method is an ideal method for creating composite coatings due to advantages such as the elimination of casting defects [2].

Metal-matrix composites (MMCs) have attracted the attention of industries such as military, transportation, and aircraft manufacturing because

Corresponding author: Hamed JAMSHIDI AVAL, Tel: +98-11-35501808, Fax: +98-11-35501800, E-mail: h.jamshidi@nit.ac.ir
DOI: 10.1016/S1003-6326(23)66165-5

of their properties. Like other composites, they are composed of two or more components that are essential in determining their properties. Depending on the application of the composite, the matrix that consists of pure metal or alloy and additive particles can be ceramic or metal [3−6]. Although metal matrix composites reinforced by ceramics have high strength and wear resistance, their low thermal expansion coefficient and toughness limit their use where high strength and toughness are required. In these conditions, MMCs reinforced by metal particles are a viable option. The type and amount of reinforcing particles and their compatibility with the crystal structure of the substrate are essential in the mechanical properties of the coating. The similarity in the cell structure of the matrix and reinforcing particles prevents debonding at the interface [7]. Since the production of MMCs with low weight and high mechanical properties is essential, metals such as aluminum receive much attention. Aluminum and its alloys are among the most widely used engineering materials and are good choices as a matrix material in metal matrix composites due to their high specific strength, wear resistance, fatigue and corrosion resistance, and high electrical and thermal conductivity [8].

A few studies have been conducted on the fabrication of composite coatings by FS. SHARMA et al [9] succeeded in coating the reinforced aluminum composite with 5−10 nm graphene particles on the surface of AA6061 aluminum alloy by FS. They observed that with increasing the percentage of graphene, the hardness decreased in the coated samples. Also, the coefficient of friction of the coating applied with graphene particles compared to the substrate has decreased by 26.76%. In another study, REDDY et al [10] produced an AA2124 composite coating reinforced with silicon carbide (SiC) particles on the surface of A356 aluminum alloy to improve corrosion and wear resistance. Under pressure and SPD during the process, the SiC particles broke and became smaller particles. Investigations reported a uniform distribution of SiC particles in the coating. OLIVEIRA et al [11] coated AA6351 aluminum-alloy reinforced with Al_2O_3 particles by FS on the surface of AA5052 aluminum alloy. They observed that after the coating process, the grain size became 48% smaller than the consumable rod due to SPD and recrystallization. GANDRA et al [12] investigated the effect of reinforcing particle size and number of holes on the FS of AA6082−SiC composite multilayer coating on AA2024 aluminum alloy substrate. In the study of wear resistance of samples containing reinforcing particles and samples without, it was observed that the presence of SiC particles prevents the coating from layering and thus increases its wear resistance. NAKAMA et al [13] coated the AA6061−Al_2O_3 composite on the AA6061 aluminum alloy substrate by FS. It was observed that although the coating efficiency increases with increasing traverse speed, the coating efficiency decreases with increasing the amount of reinforcement.

In all these studies, the addition of ceramic particles to the consumable rod increased the hardness and strength of the coating. However, composites reinforced by ceramic particles have low toughness, and its formability is highly reduced. Metal particles are added in the fabrication of the composite coating to solve this problem [14,15]. The type, size, and amount of reinforcing particles are highly effective in increasing the mechanical properties of MMCs, and the intermetallic compounds produced during the process in the composite increase the strength. Copper is an ideal reinforcing particle in the aluminum matrix. Due to its reasonable price, high wear resistance, its crystalline structure similar to aluminum, and the creation of high-strength intermetallic compounds such as Al_2Cu [16], it can improve the mechanical properties of aluminum matrix composites. In this study, the effect of the rotational speed of the coating process on the microstructure, mechanical properties, and wear resistance of the composite coating by applying an AA5083 aluminum alloy matrix reinforced with copper particles through the FS process, is investigated.

2 Experimental

This research used an AA1050 aluminum sheet with a thickness of 4 mm as the substrate and an AA5083 aluminum alloy rod with a diameter of 20 mm as the consumable rod. Table 1 lists the chemical compositions of the substrate and the consumable rod. Copper powder with a purity of 99% and size of 5−60 μm was used as a reinforcing agent. Two holes were created according to Fig. 1 to apply copper powder to the cross-section of the

consumable rod. 10 wt.% of copper powder was applied to the consumable rod through drilled holes with a diameter of 3 mm and a length of 60 mm. After drilling, the copper powder was applied to the holes. The coated samples were named according to Table 2. FS was performed using the traverse speed of 100 mm/min, axial feeding rate of 200 mm/min, and rotational speeds of 400, 600, 800, 1000, and 1200 r/min.

Table 1 Chemical compositions of AA1050 substrate and AA5083 consumable rod (wt.%)

Alloy	Si	Fe	Mg	Mn	Cu	Al
AA1050	0.07	0.28	0.01	0.02	0.05	Bal.
AA5083	0.31	0.29	4.23	0.58	0.08	Bal.

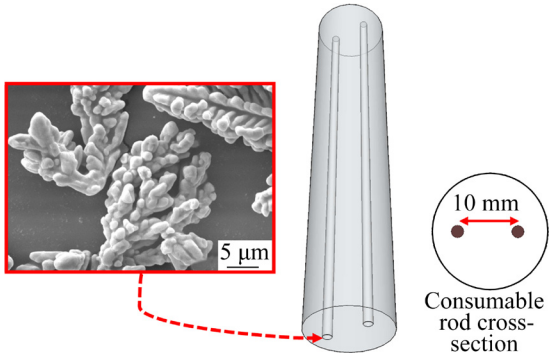

Fig. 1 Schematic view of holes drilled in consumable rod cross section

After applying the coating, different samples were extracted to evaluate the microstructure, mechanical properties, and wear properties of the coatings (Fig. 2). After grinding and polishing, metallographic samples were etched using Poulton's reagent (2 mL HF, 3 mL HCl, 20 mL HNO_3, and 175 mL H_2O). The microstructure of the coating was studied using an optical microscope and scanning electron microscopy (SEM) equipped with an energy-dispersive X-ray (EDS) detector. A linear intercept technique (ASTM E112–96) was used to determine the grain sizes. For measuring grain size at advancing, retreating, and center of coatings, at least four images were used. The image analysis was performed using Clemex image analysis software. Hardness and shear tests were used to evaluate the mechanical properties of the coating. The hardness test was performed according to the ASTM E92 micro-Vickers hardness test with a 0.98 N load and a 10 s dwell duration. The shear test was performed based on the method presented in ASTM A264 [17] and a speed of 1 mm/min. The shear strength was calculated by dividing the maximum load on the coating/substrate interface area during the shear test. The wear properties of the coating were investigated based on the standard

Table 2 Coated samples labeling

Sample	Rotational speed/ ($r \cdot min^{-1}$)	Traverse speed/ ($mm \cdot min^{-1}$)	Axial feeding rate/ ($mm \cdot min^{-1}$)
C-400	400	100	200
C-600	600	100	200
C-800	800	100	200
C-1000	1000	100	200
C-1200	1200	100	200
W-600*	600	100	200
W-800*	800	100	200
W-1000*	1000	100	200

* The coated samples without copper reinforcement

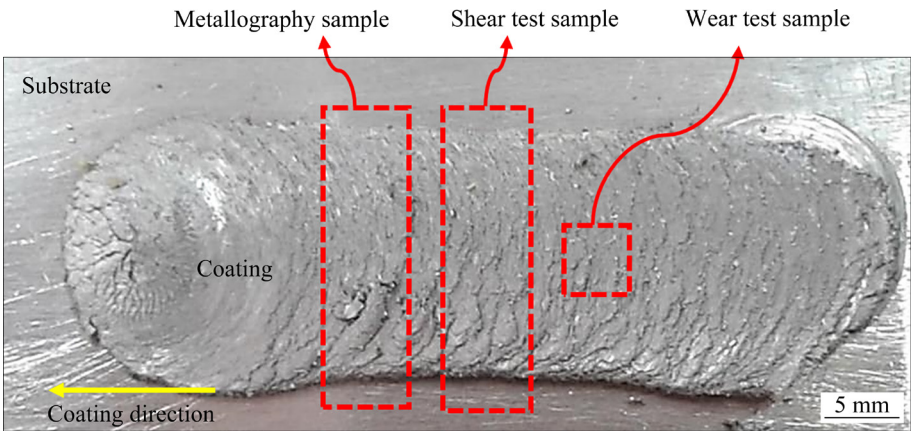

Fig. 2 Microstructural examination, shear test and wear test samples extraction position

ASTM G99−05 and at a distance of 2000 m. The pin-on-disk (POD) test was employed to evaluate the samples' wear properties under ASTM G99—05. The POD test was conducted at a load of 20 N and a linear speed of 50 cm/s on a counterface disc made of 60 HRC AISI/SAE 52100 steel. The measurement process of the mechanical and wear properties was repeated three times in each condition to ensure the reproducibility of the results. The distribution coefficient (DF) of the reinforcing particles based on Refs. [18,19] was obtained by dividing the standard deviation of reinforcing particles' surface fractions by their average.

3 Results and discussion

3.1 Macrostructure examination

Figure 3 shows the effect of rotational speed on the cross-section and top surface morphologies of the created coatings. As can be seen, no coating was applied to the surface of the substrate at the rotational speeds of 400 and 1200 r/min. As Fig. 3 shows, at the rotational speed of 400 r/min, the consumable rod was tilted due to vertical force, and the process could not be continued. Although at the rotational speed of 1200 r/min, the heat input was high, it was not possible to deposit the material on the substrate due to the high shear stress created at the interface of the consumable rod and the substrate.

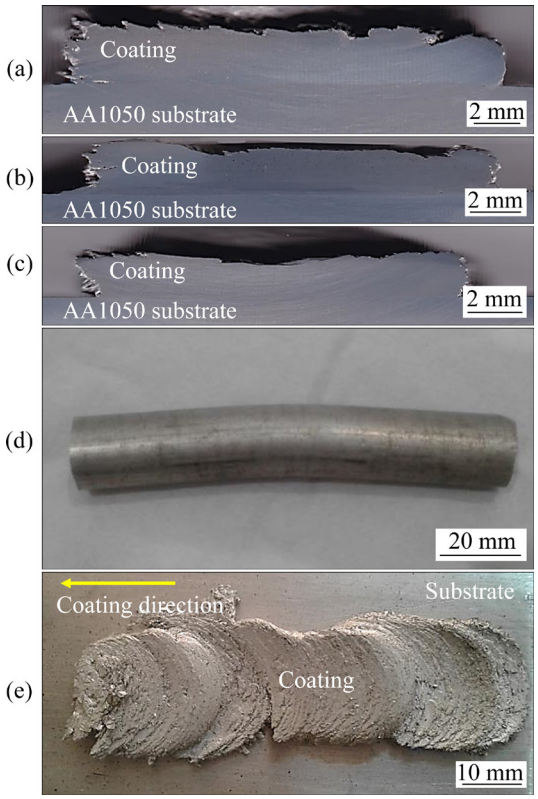

Fig. 3 Morphologies of cross-section of composite coated samples ((a) C-600, (b) C-800, (c) C-1000), consumable rod during coating of Sample C-400 (d), and top surface of Sample C-1200 (e)

There, as shown in the image, the coating on the substrate surface was irregular and scattered. At rotational speeds of 600, 800, and 1000 r/min, a uniform, defect-free coating was formed. Temperature measurement at the tip of the consumable rod using a laser thermocouple showed a temperature of 340, 364, and 389 °C at the created coating with a rotational speed of 600, 800, and 1000 r/min, respectively. As can be seen, the temperature of the tip of the consumable rod increases with increasing rotational speed. In this case, the plastic deformation of the consumable rod occurs more easily. As explained later in the microstructure section, with increasing the rotational speed, the dispersion of copper powder particles is improved, and the agglomeration of copper powder is reduced. Measurements of the coating dimensions (Fig. 4) showed that the width and the effective thickness of the coating decreased with increasing rotational speed. Increasing the plastic deformation capability of the material will cause the deposited material to spread more widely under the axial force, and the thickness of the coating will decrease under the forging force of the consumable rod. However, although the coating width increases, the effective coating width is decreased due to higher shear force in the interface. The coating efficiency was calculated using the procedure in Ref. [2], and the efficiency in the

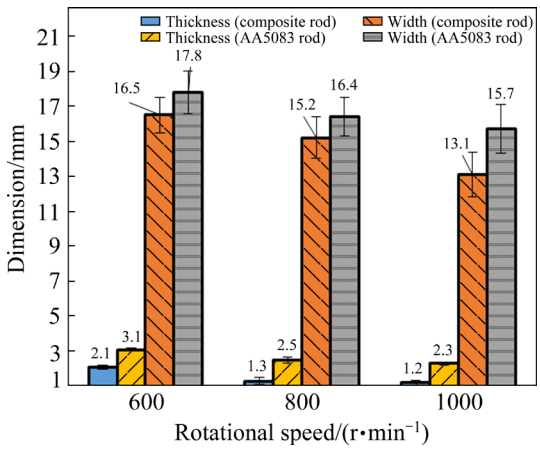

Fig. 4 Effect of traverse speed on width and thickness of coating created with AS and SS consumable rods

coatings with rotational speeds of 600, 800, and 1000 r/min was 31%, 28%, and 25%, respectively. Due to the reduction of effective dimensions of the coating, reducing the efficiency of the coating by increasing the rotational speed is not unexpected.

3.2 Microstructure analysis

Figure 5 shows the optical microscopy image of the central zone of the coatings. The microstructure in coatings is generally uniform. The microstructure containing equiaxed grains is formed as a result of dynamic recrystallization during the FS. The characteristic feature of friction surfacing is a combination of large strain, high temperature, and high strain rate. The effect of the temperature and the strain rate on the structural behavior is conventionally described in terms of the Zener−Hollomon parameter [20]. In the friction stir-based processes, the Zener−Hollomon parameter is relatively small [21], meaning that the structure restoration processes, including grain-boundary migration, may readily occur. In aluminum alloys with relatively high stacking fault energy, the large strain frequently leads to grain subdivision [22], which may be considered a continuous recrystallization type. Indeed, the special nature of the friction surfacing process enables the simultaneous occurrence of continuous and discontinuous recrystallizations. As shown in Fig. 6, the average grain size of coating without copper reinforcement decreased from (5.3±0.2) to (3.6±0.3) μm by increasing the rotational speed from 600 to 1000 r/min. However, there were not many changes in grain size in various areas of the coating. The lack of difference in grain size at different coating zones could be due to the high heat sink of aluminum and the slight difference in the plastic strain of different coating zones [23,24]. Also, the average grain size of the coating containing copper reinforcement decreased from (2.0±0.1) to (0.9±0.2) μm by increasing the rotational speed from 600 to 1000 r/min. The two factors of temperature and plastic strain affect the formation of recrystallized grains [25]. These two factors inversely affect the grain size, so with decreasing temperature and increasing plastic strain, the recrystallized grain size decreases. According to Ref. [26] and the geometric and process parameters of different coatings, the plastic strain rate in the coatings created with rotational speeds of 600, 800,

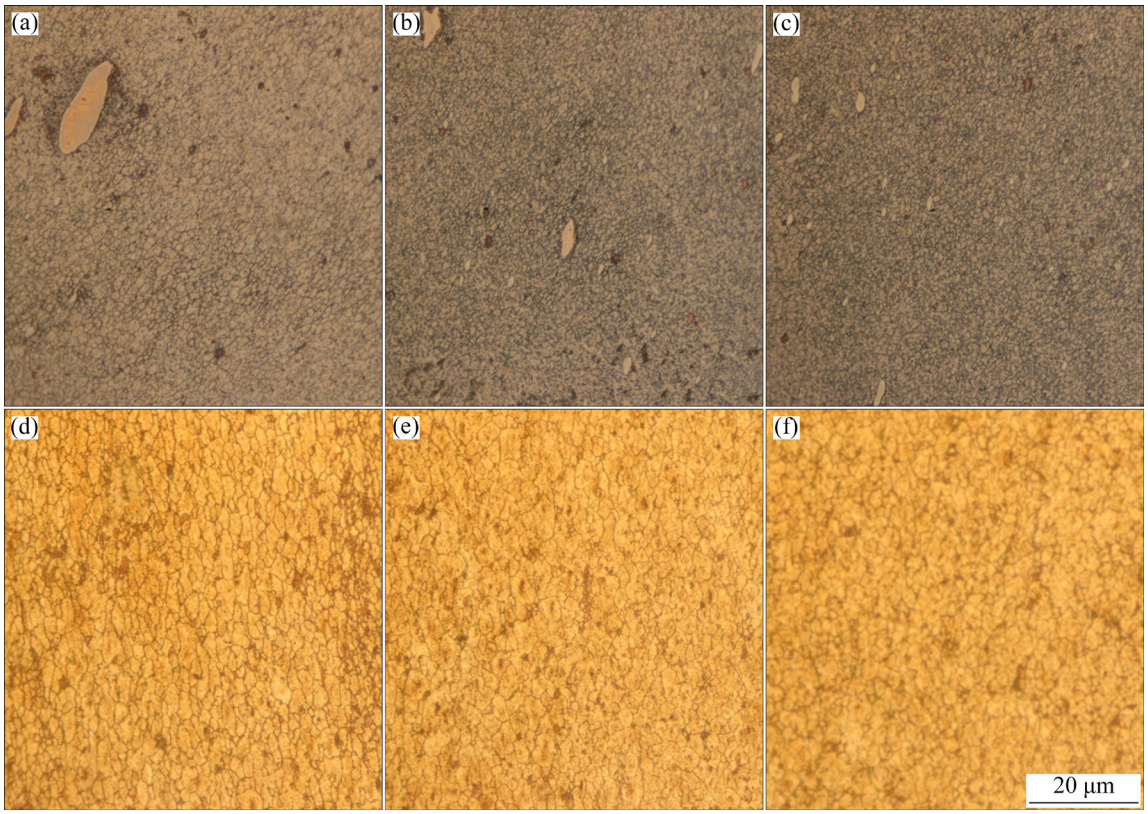

Fig. 5 Microstructure at center zone of coated samples: (a) Sample C-600; (b) Sample C-800; (c) Sample C-1000; (d) Sample W-600; (e) Sample W-800; (f) Sample W-1000

and 1000 r/min was 1310, 1450, and 1565 s^{-1}, respectively. Based on the results of temperature and plastic strain, with increasing the rotational speed, temperature changes tend to increase grain size, and plastic strain changes tend to reduce grain size. Since the grain size decreases with increasing rotational speed, the effect of plastic strain rate on the grain size changes is likely predominant.

On the other hand, it is essential to note that according to Fig. 7, the distribution factor of copper particles in the coating changes from 0.43 to 0.38 with increasing rotational speed. Reducing the distribution coefficient by increasing the rotational speed means more uniform distribution of copper-rich particles. Therefore, with a more uniform distribution of copper-rich particles, the particle stimulated nucleation (PSN) mechanism becomes more active and can cause more nucleation in the coating.

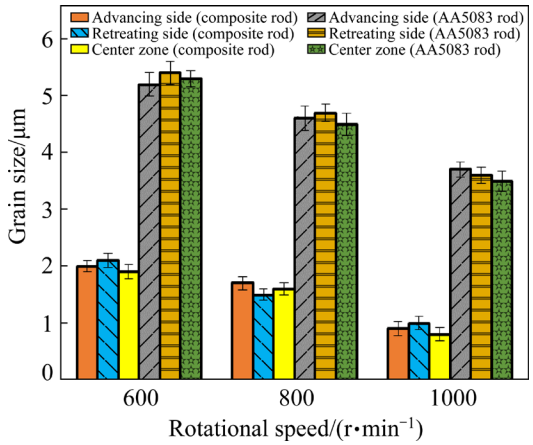

Fig. 6 Effect of consumable rod rotational speed on grain size of coating containing copper (composite rod) and without copper (AA5083 rod)

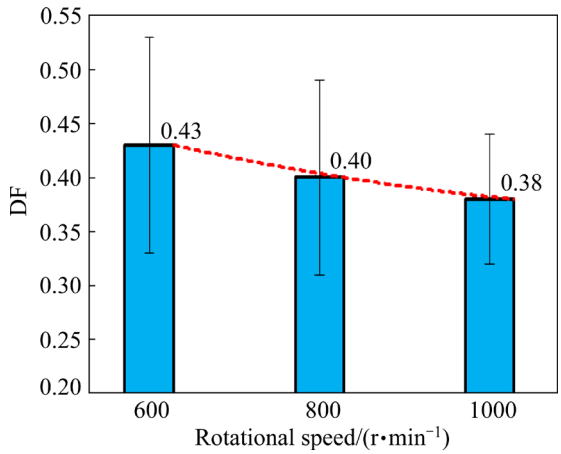

Fig. 7 Effect of consumable rod rotational speed on distribution factor (DF)

Figure 8 shows the microstructure of various coatings evaluated by scanning electron microscopy. According to the EDS chemical analysis (Fig. 9), Mg-rich, Fe-rich, and Cu-rich precipitates and secondary phase particles are observed in the microstructure of the coatings. As can be seen, the main difference between the coatings is the distribution and the nature of the interface layers in the copper-rich particles. As the rotational speed increases, while the copper-rich particles become smaller, mainly copper-rich particles are formed as $CuAl_2$ intermetallic compounds. By decreasing the

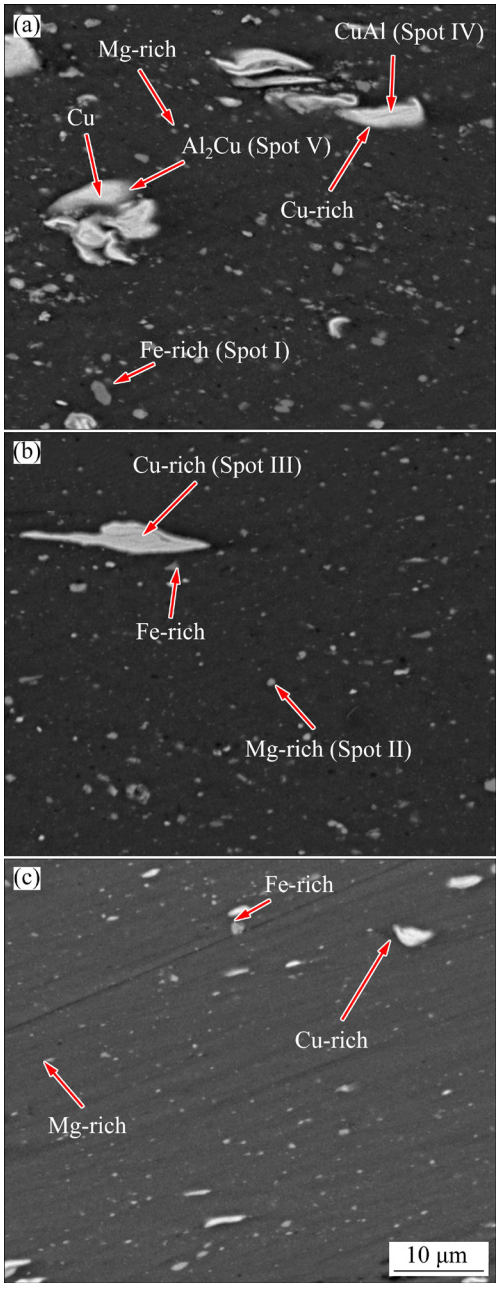

Fig. 8 SEM micrograph of precipitates and second-phase particles of coated samples: (a) Sample C-600; (b) Sample C-800; (c) Sample C-1000

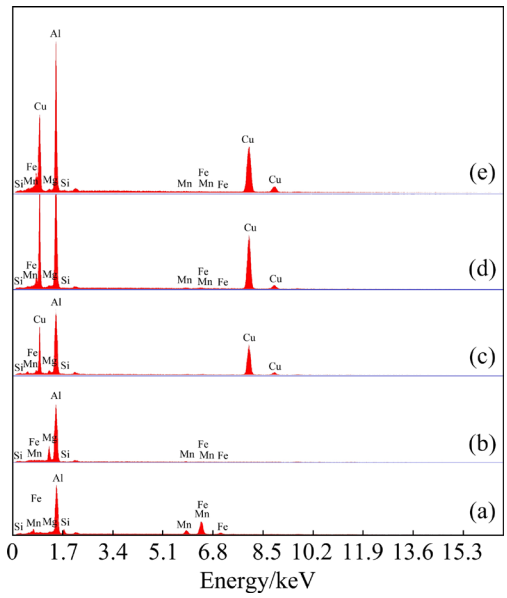

Fig. 9 EDS analysis result of precipitates and secondary phase particles in Fig. 8: (a) Fe-rich (Spot I); (b) Mg-rich (Spot II); (c) Cu-rich (Spot III); (d) AlCu (Spot IV); (e) Al_2Cu (Spot V)

rotational speed and increasing the size of copper-rich particles, it is observed that while changing the morphology of these particles from equiaxed to large aspect ratio one, different layers are formed at the interface between these particles and the aluminum matrix. As the particle size increases, the central part of the particles remains unreacted, and by moving towards the aluminum matrix, CuAl and $CuAl_2$ intermetallic compounds are formed. The amount of copper dissolved in the aluminum matrix in the coated sample with a rotational speed of 600, 800, and 1000 r/min is 8, 9, and 6 wt.%, respectively. There is no significant difference in the amount of dissolved copper in the aluminum matrix of different samples. Therefore, it can be said that despite the high temperature and plastic strain during the process, copper cannot diffuse from copper-rich particles into the aluminum matrix and dissolve in it. This phenomenon prevents the formation of precipitation in the matrix alloy. According to Refs. [1,27,28], homogenization treatment and helping to dissolve copper in the matrix may create precipitation capability. Figure 10 shows the result of X-ray diffraction of different coatings to investigate the phases formed in the coating. Except for the coated sample with a rotational speed of 1000 r/min, no peak related to intermetallic compounds appeared in other samples. Although according to the SEM results, the intermetallic compound was formed at the interface of the copper-rich particles, the absence of these compounds in the XRD results is probably due to the small amounts of these compounds. Based on the XRD pattern of the coated sample with a rotational speed of 1000 r/min, the formation of the $CuAl_2$ intermetallic compound, also reported in the SEM results, is confirmed.

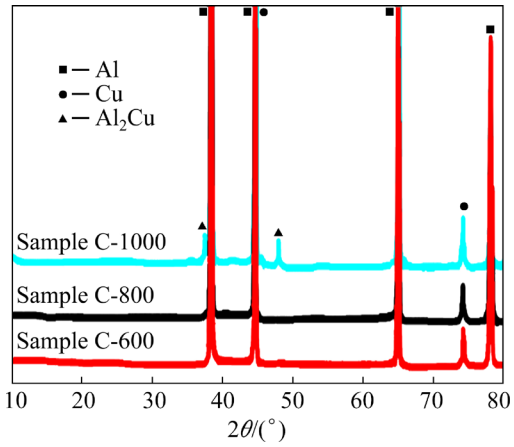

Fig. 10 XRD patterns of different coated samples

3.3 Mechanical properties

Figure 11 shows the hardness changes perpendicular to the interface of the coating/substrate. In all coated samples, except the coated sample with a rotational speed of 1000 r/min, the hardness changes are non-uniform. So, the hardness increases from a minimum value by moving towards the center of the coating and decreases again. In the coated sample with a rotational speed of 1000 r/min, the hardness changes are more uniform. However, in the two coated samples with rotational speeds of 600 and 800 r/min, non-uniform hardness changes are due to the non-uniform distribution of copper-rich particles in the coating. This is not unexpected due to the high density of these particles in the central zone of the coating. The average hardness and shear strength of the coatings are shown in Fig. 12. As can be seen, the values of hardness and shear strength increase with increasing rotational speed from 600 to 1000 r/min. The noteworthy point in these images is the deviation of the hardness and the shear strength of the coating, which decreases with increasing rotational speed. Another influential factor in strengthening is modulus strengthening.

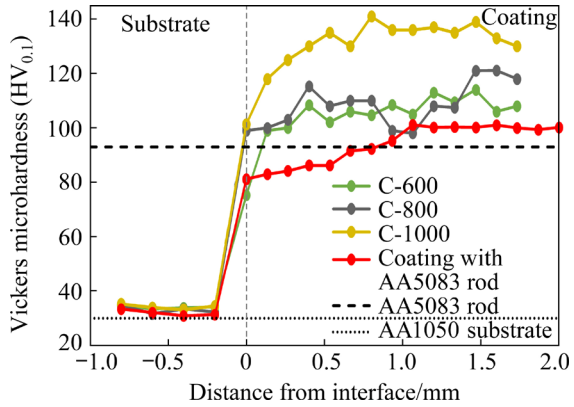

Fig. 11 Variation of hardness profile perpendicular to coating/substrate interface

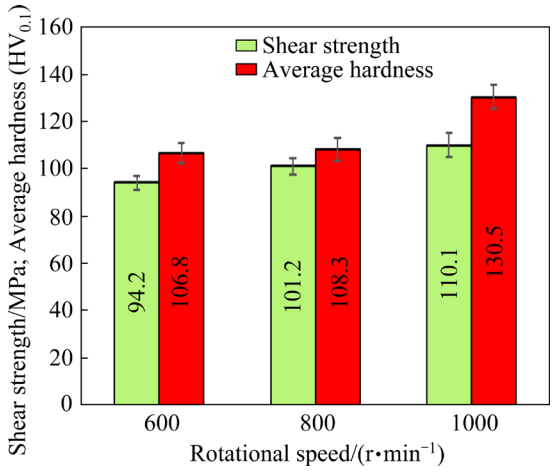

Fig. 12 Variation of hardness and interface shear strength of coated samples versus consumable rotational speed

The energy of dislocation is a function of the shear modulus of the lattice within which it resides. As a dislocation moves from the matrix into a particle with a different shear modulus, a change occurs in dislocation energy, and hence, an interaction force appears between the dislocation and the particle [29]. As the elastic modulus of aluminum−copper-base intermetallic compound [30] is higher than that of aluminum, it is expected that reinforcement through elastic modulus contributes much to the strength of the composite coating, especially when the distribution of copper-rich particles in the microstructure is uniform. The reinforcing particles affect the change in the density of dislocations in two ways: local deformation around the particles and the difference in the coefficient of thermal expansion of the reinforcing particles and the matrix. Due to the severe plastic deformation around the relatively large reinforcing particles, deformation zones are formed near the particles due to the local rotation of the lattice there. These areas contain a complex structure of dislocations. The size and distribution of these areas depend first on the applied strain and particle size and then on the shape and quality of the particle and the matrix interface [25]. The difference in the coefficient of thermal expansion of the reinforcing particles and the matrix causes the formation of dislocations near the interface. This is due to the creation of multidimensional thermal stresses during cooling from the deformation temperature [31,32].

Figure 13 shows the force−displacement diagram of different coatings. The maximum force required to separate the bond between the coating and the substrate increases with increasing rotational speed. In this sample, the increase in heat input and plastic strain at the maximum rotational speed has possibly increased the diffusion and interaction of the substrate and coating, leading to a stronger bond. A more uniform hardness profile and microstructure of the coating created with a rotational speed of 1000 r/min can prevent stress concentration and sharp stress changes and strengthen the joint. Figure 14 shows the fracture surface morphology of different samples. The presence of smooth, dimple-free surfaces in samples with speeds of 600 and 800 r/min confirms lower bond strength and stress concentration in the interface.

3.4 Wear resistance

Figure 15 compares the results of friction coefficient and wear rate of different coatings with

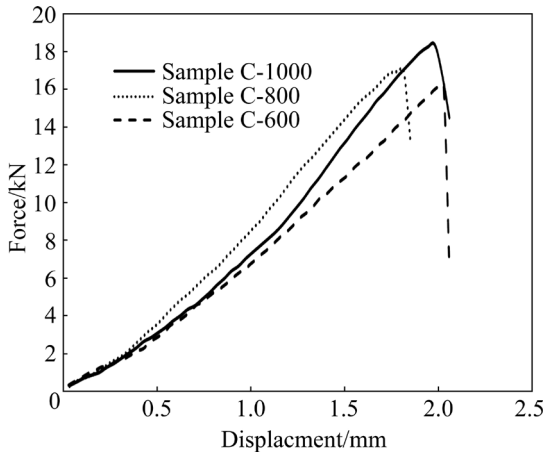

Fig. 13 Force−displacement diagram of different coatings

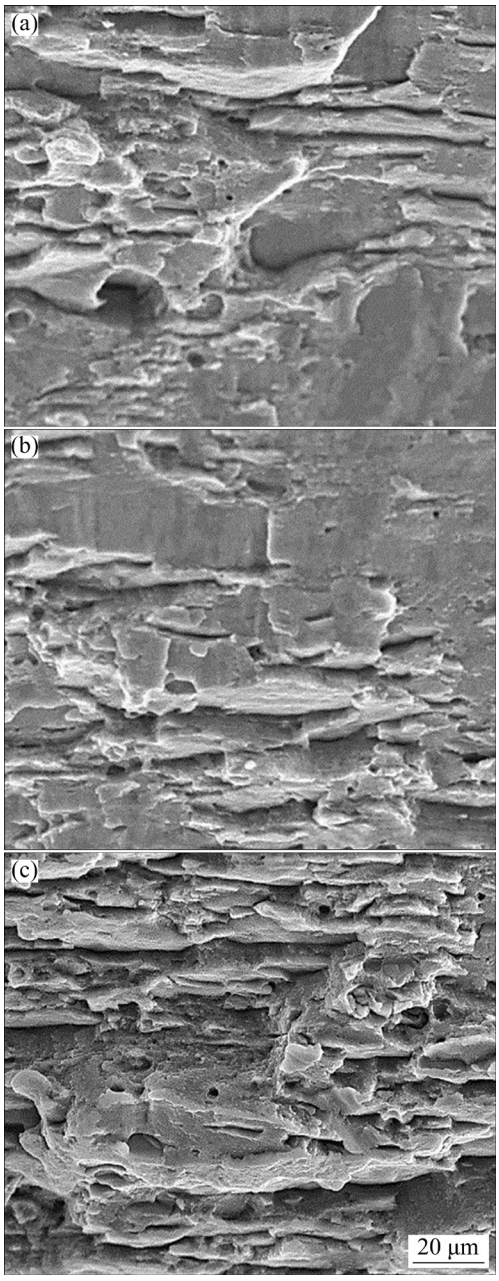

Fig. 14 SEM image of fracture surface: (a) Sample C-600; (b) Sample C-800; (c) Sample C-1000

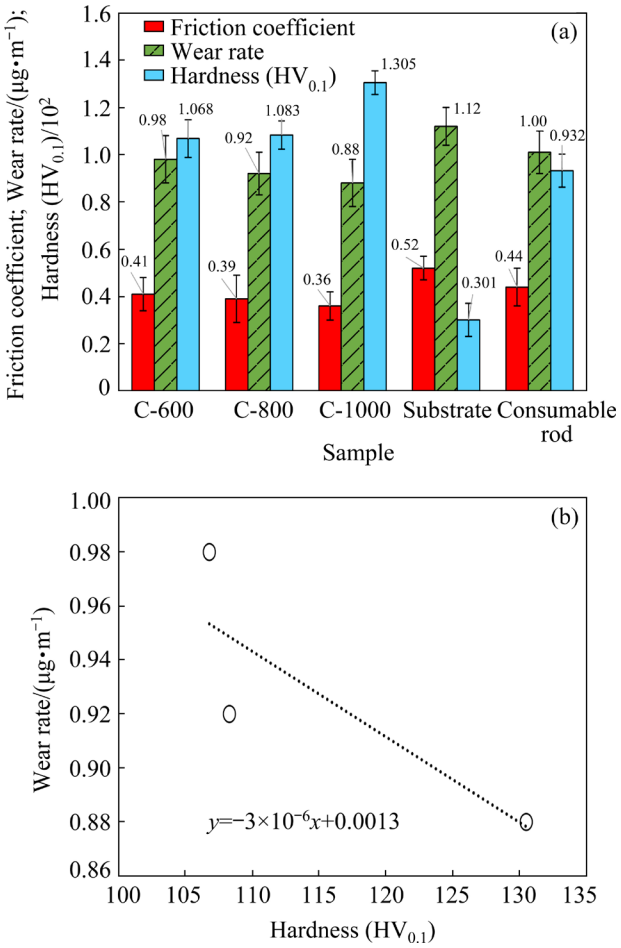

Fig. 15 Wear rate, friction coefficient and hardness of different samples (a); Wear rate versus hardness curve of coatings (b)

the values related to the substrate and the consumable rod. The coefficients of friction of the AA1050 substrate and the consumable rod are 0.52 and 0.44, respectively. As can be seen, applying the coating with each of the rotational speeds of 600, 800, and 1000 r/min results in a lower wear rate and coefficient of friction than those of the consumable rod and substrate. There is also a direct relationship between the wear rate and the change in hardness of different coatings. As the hardness of the coating grows, the wear resistance of the coating increases. The linear relation is predicted for the wear rate and hardness of coatings. It is noteworthy that with higher deviation in hardness results, the data on wear rate and coefficient of friction also show more deviation. This shows that the microstructure and distribution of particles affect not only the hardness and mechanical properties of the coating but also the wear behavior.

Figure 16 shows the worn surface morphology of different samples. Adhesive wear has a severe form characterized by high wear rates and a large unstable friction coefficient. All metals show a strong tendency to adhere to contact with another solid, but there are significant differences between particular elements. It has been found experimentally that metals such as aluminum, with a face-centered cubic structure, show stronger adhesion than other crystal structures due to a higher degree of plastic deformation between asperities [33,34]. The groove formation mechanism involves plowing the softer substrate

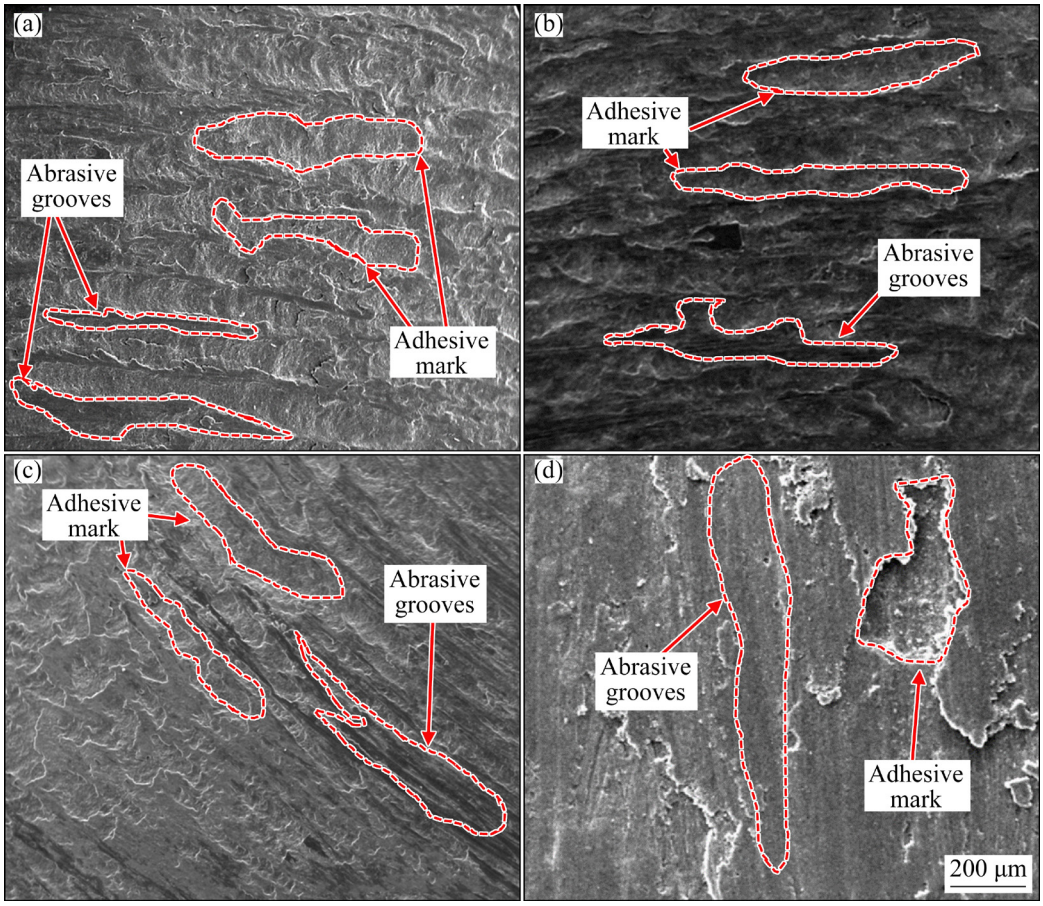

Fig. 16 SEM micrograph of worn surface of coated samples and substrate: (a) Sample C-600; (b) Sample C-800; (c) Sample C-1000; (d) Substrate

material by work-hardened transfer particles [35]. Plowing is a very inefficient cutting method that can lead to crack formation on the worn surface due to high tensile stresses. The formation of grooves on worn surfaces is frequently observed when adhesive wear occurs. Figure 16 indicates that evidence for both adhesive and abrasive wear mechanisms can be found in the worn surface of samples. As the hardness in the coating decreases, the contribution of the adhesive wear mechanism increases, while as the hardness of the coating increases, the depth and width of the grooves created at the worn surface decrease. The abrasive wear mechanism observed in the worn surface is of a two-body type. The presence of aluminum oxide particles on the worn surface indicates the occurrence of three-body type wear. The aluminum pieces separated from the surface can be oxidized with increasing temperature during the wear test, causing the oxide pieces to move into the grooves created during wear, forming a protective layer on the pin surface, thus reducing the wear rate.

4 Conclusions

(1) The width and the effective thickness of the coating decreased with increasing rotational speed. Also, by increasing the rotational speed of the consumable rod from 600 to 1000 r/min, the coating efficiency decreases from 31% to 25%.

(2) Due to the high heat sink of the substrate and the slight difference in plastic strain, the grain size at different zones of coatings is not varied. However, by increasing the rotational speed from 600 to 1000 r/min, the average grain size decreases from (2.0±0.1) to (0.9±0.2) μm.

(3) The distribution coefficient of copper particles in the coating changes from 0.43 to 0.38 with increasing rotational speed from 600 to 1000 r/min. Reducing the distribution coefficient by increasing the rotational speed means more uniform distribution of copper-rich particles.

(4) By decreasing the rotational speed, the morphology of copper-rich particles changes from

equiaxed to large aspect ratio one, and different layers are formed at the interface between these particles and the aluminum matrix.

(5) As the particle size increases, the central part of the particles remains unreacted, and by moving towards the aluminum matrix, CuAl and $CuAl_2$ intermetallic compounds are formed.

(6) The deviation of the hardness and the shear strength of the coating decreases with increasing rotational speed. Also, coating with a rotational speed of 1000 r/min results in the maximum load (18.4 kN) needed for debonding the coating from the substrate.

(7) With decreasing hardness in the coating, the contribution of the adhesive wear mechanism increases.

References

[1] PIRHAYATI P, JAMSHIDI AVAL H. Microstructural characterization and mechanical properties of friction surfaced AA2024−Ag composites [J]. Transactions of Nonferrous Metals Society of China, 2020, 30(7): 1756−1770.

[2] GANDRA J, KROHN H, MIRANDA R, VILAÇA P, QUINTINO L, DOS SANTOS J. Friction surfacing—A review [J]. Journal of Materials Processing Technology, 2014, 214: 1062−1093.

[3] UYYURU R, SURAPPA M, BRUSETHAUG S. Tribological behavior of Al−Si−SiC_p composites/automobile brake pad system under dry sliding conditions [J]. Tribology International, 2007, 40(2): 365−373.

[4] NIE Q Q, CHEN G H, WANG B, YANG L, TANG W M. Process optimization, microstructures and mechanical/ thermal properties of Cu/Invar bi-metal matrix composites fabricated by spark plasma sintering [J]. Transactions of Nonferrous Metals Society of China, 2021, 31(10): 3050−3062.

[5] VICTOR CHRISTY J, ISMAIL MOURAD A H, SHERIF M M, SHIVAMURTHY B. Review of recent trends in friction stir welding process of aluminum alloys and aluminum metal matrix composites [J]. Transactions of Nonferrous Metals Society of China, 2021, 31(11): 3281−3309.

[6] GUAN Z P, LI M Y, XIA K X, LI Z G, GAO D, ZHAO P, MA P K, SONG J W. Microstructure, mechanical properties and wear resistance of SiC_p/AZ91 composite prepared by vacuum pressure infiltration [J]. Transactions of Nonferrous Metals Society of China, 2022, 32(1): 104−121.

[7] SPRING D W, PAULINO G H. Computational homogenization of the debonding of particle reinforced composites: The role of interphases in interfaces [J]. Computational Materials Science, 2015, 109: 209−224.

[8] MOSISA E, BAZHIN V Y, SAVCHENKOV S. Review on nano particle reinforced aluminum metal matrix composites [J]. Research Journal of Applied Sciences, 2016, 11(5): 188−196.

[9] SHARMA A, SAGAR S, MAHTO R P, SAHOO B, PAL S K, PAUL J. Surface modification of Al6061 by graphene impregnation through a powder metallurgy assisted friction surfacing [J]. Surface and Coatings Technology, 2018, 337: 12−23.

[10] REDDY G M, RAO K S, MOHANDAS T. Friction surfacing: Novel technique for metal matrix composite coating on aluminium–silicon alloy [J]. Surface Engineering, 2009, 25(1): 25−30.

[11] OLIVEIRA P H F, GALVIS J C, DE PAULA MARTINS J, CARVALHO A L M. Application of friction surfacing to the production of aluminum coatings reinforced with Al_2O_3 particles [J]. Materials Research, 2017, 20: 603−620.

[12] GANDRA J, VIGARINHO P, PEREIRA D, MIRANDA R, VELHINHO A, VILAÇA P. Wear characterization of functionally graded Al−SiC composite coatings produced by friction surfacing [J]. Materials & Design, 2013, 52: 373−383.

[13] NAKAMA D, KATOH K, TOKISUE H. Fabrication of 6061 aluminum alloy/$A1_2O_3$ particle composites by friction surfacing [J]. Journal of Japan Institute of Light Metals, 2008, 58(7): 299−304.

[14] KUMAR V M, DEVI C N. Evaluation of mechanical characteristics for aluminum-copper metal matrix composite [J]. Research Journal of Engineering Sciences, 2014, 2278: 9472.

[15] RAHMATI Z, JAMSHIDI AVAL H, NOUROUZI S, JAMAATI R. Effect of copper reinforcement on the microstructure, macrotexture, and wear properties of a friction-surfaced Al−Cu−Mg coating [J]. Surface and Coatings Technology, 2022, 438: 128380.

[16] MAHMOUD E R I, AL-QOZAIM A M A. Fabrication of in-situ Al−Cu intermetallics on aluminum surface by friction stir processing [J]. Arabian Journal for Science and Engineering, 2016, 41(5): 1757−1769.

[17] HORSTMAN R, PETERS K A, MELTZER R L, VIETH M B, BLICKENSDERFER R, BURRUS J M. A multistep shear test for bond strength of claddings [J]. Journal of Testing and Evaluation, 1984, 12(1): 3−12.

[18] YUAN X, JIA L, BA Z, SHENG X, XIONG Z, editors. Quantitative assessment of uniformity in particle distribution [C]//International Conference on Intelligent Robotics and Applications. Busan, South Korea, 2013.

[19] AKHLAGHI F, LAJEVARDI A, MAGHANAKI H. Effects of casting temperature on the microstructure and wear resistance of compocast A356/SiC_p composites: A comparison between SS and SL routes [J]. Journal of Materials Processing Technology, 2004, 155: 1874−1880.

[20] SUHUDDIN U, MIRONOV S, KROHN H, BEYER M, DOS SANTOS J. Microstructural evolution during friction surfacing of dissimilar aluminum alloys [J]. Metallurgical and Materials Transactions A, 2012, 43(13): 5224−5231.

[21] MORISHIGE T, HIRATA T, TSUJIKAWA M, HIGASHI K. Comprehensive analysis of minimum grain size in pure aluminum using friction stir processing [J]. Materials Letters, 2010, 64(17): 1905−1908.

[22] HANSEN N, JENSEN D J. Development of microstructure in FCC metals during cold work [J]. Philosophical Transactions of the Royal Society of London Series A: Mathematical, Physical and Engineering Sciences, 1999, 357(1756): 1447−1469.
[23] BARARPOUR S M, JAMSHIDI AVAL H, JAMAATI R. Modeling and experimental investigation on friction surfacing of aluminum alloys [J]. Journal of Alloys and Compounds, 2019, 805: 57−68.
[24] RAHMATI Z, JAMSHIDI AVAL H, NOUROUZI S, JAMAATI R. Effects of pre-heat treatment of the consumable rod on the microstructural and mechanical properties of the friction surfaced Al−Cu−Mg alloy over pure aluminum [J]. Surface and Coatings Technology, 2021, 410: 126954.
[25] HUMPHREYS F J, HATHERLY M. Recrystallization and related annealing phenomena [M]. Elsevier, 2012.
[26] EHRICH J, ROOS A, KLUSEMANN B, HANKE S. Influence of Mg content in Al alloys on processing characteristics and dynamically recrystallized microstructure of friction surfacing deposits [J]. Materials Science and Engineering A, 2021, 819: 141407.
[27] BARARPOUR S M, JAMSHIDI AVAL H, JAMAATI R. Effects of Zn powder on alloying during friction surfacing of Al−Mg alloy [J]. Journal of Alloys and Compounds, 2020, 818: 152823.
[28] PIRHAYATI P, JAMSHIDI AVAL H. Effect of post-heat treatment on friction surfaced Al−Cu−Mg alloy coating containing Ag [J]. Surface and Coatings Technology, 2020, 397: 125984.
[29] MCQUEEN H, BAILON J P, DICKSON J. Strength of metals and alloys (ICSMA 7) [C]//Proceedings of the 7th International Conference on the Strength of Metals and Alloys. Montreal, Canada: Elsevier, 2016.
[30] ZHOU W, LIU L J, LI B L, SONG Q G, WU P. Structural, elastic, and electronic properties of Al−Cu intermetallics from first- principles calculations [J]. Journal of Electronic Materials, 2009, 38(2): 356−364.
[31] MOHAMADIGANGARAJ J, NOUROUZI S, JAMSHIDI AVAL H. The effect of heat treatment and cooling conditions on friction stir processing of A390−10wt.%SiC aluminium matrix composite [J]. Materials Chemistry and Physics, 2021, 263: 124423.
[32] MEIJER G, ELLYIN F, XIA Z. Aspects of residual thermal stress/strain in particle reinforced metal matrix composites [J]. Composites Part B: Engineering, 2000, 31(1): 29−37.
[33] SIKORSKI M E. Correlation of the coefficient of adhesion with various physical and mechanical properties of metals [J]. Journal of Basic Engineering, 1963, 85(2): 279−285.
[34] STACHOWIAK G W, BATCHELOR A W. Engineering tribology [M]. 4th ed. Butterworth−Heinemann, 2013.
[35] KOMVOPOULOS K, SAKA N, SUH N. The mechanism of friction in boundary lubrication [J]. Journal of Tribology, 1985, 107(4): 452−462.

AA1050 表面 Al−Mg−$Cu_{(p)}$复合涂层的力学和摩擦学性能

Hamed JAMSHIDI AVAL

Department of Materials Engineering, Babol Noshirvani University of Technology,
Shariati Avenue, Babol 47148-71167, Iran

摘　要：研究添加铜粉和改变耗材转速对 AA1050 铝合金基体上摩擦堆焊 Al−Mg 涂层力学和摩擦学性能的影响。铜粉是通过在耗材的横截面上钻孔的方式嵌入的。用光学显微镜和电子显微镜研究涂层的显微组织，用剪切实验研究涂层的力学性能。结果表明，当耗材转速从 600 r/min 增加到 1000 r/min 时，铜粉分布更加均匀，铜粉团聚现象减少，涂层的平均晶粒尺寸从(2.0±0.1) μm 减小到(0.9±0.2) μm。随着转速的增加，富铜颗粒变小，并形成 $CuAl_2$ 金属间化合物。当耗材转速从 600 r/min 增加到 1000 r/min，使涂层从基体剥离所需的最大力从 16.2 kN 增加到 18.4 kN 。转速为 600、800 和 1000 r/min 制备的涂层其磨损率分别比 AA1050 基材的低 12%、18%和 21%。

关键词：摩擦面；Al−Mg 基复合材料；铜增强体；力学性能；AA1050 基体

(Edited by Bing YANG)